文章编号:1001-9014(XXXX)XX-0001-08

DOI:10. 11972/j. issn. 1001-9014. XXXX. XX. 001

通过太赫兹近场成像技术揭示牙釉质脱矿的微观奥秘

肖 丰[1,2], 张晓秋艳[1,2], 程 立[3], 许星星[1,2], 张天宇[1,2], 唐 福[1,2], 胡 涛[3], 胡 旻[1,2]

(1. 电子科技大学,电子科学与工程学院,太赫兹中心,中国成都610054;
2. 太赫兹技术教育部重点实验室,中国成都610054;
3. 四川大学华西口腔医院口腔疾病国家重点实验室,国家口腔疾病临床研究中心,中国成都610054)

摘要:牙釉质脱矿通常发生在龋病的早期。研究牙釉质脱矿的微观机制对预防和治疗龋病具有重要意义。太赫兹技术,特别是连续波太赫兹近场扫描显微镜技术,以其纳米级分辨率在生物医学成像领域具有广阔的应用前景。此外,与传统的太赫兹时域光谱相比,便携式固体源作为发射源具有更高的功率和信噪比,更低的成本,可以获得更精确的成像。在本研究中,我们利用连续波太赫兹近场扫描显微镜系统进一步突破了传统太赫兹成像技术的分辨率限制,成功实现了纳米尺度下脱矿牙釉质的近场成像。我们敏锐地观察到,随着脱矿的加深,牙釉质的近场信号明显降低,这主要是由于介电常数的降低。这一新方法为牙釉质脱矿的微观过程提供了有价值的见解,为龋病进一步的研究和治疗奠定了基础。

关 键 词:脱矿牙釉质;近场;连续波太赫兹近场扫描显微镜

Li Cheng: dentistcl@scu.edu.cnMin Hu:hu_m@uestc.edu.cn

Illuminating the Microscopic Mysteries of Enamel Demineralization through Terahertz Near-field Imaging

Xiao Feng[1,2], Zhang Xiaoqiuyan[1,2], Cheng Li[3], Xu Xingxing[1,2], Zhang Tianyu[1,2], Tang Fu[1,2], Hu Tao[3], Hu Min[1,2]

(1. Terahertz Research Center, School of Electronic Science and Engineering, University of Electronic Science and Technology of China, Chengdu 610054, China;
2. Key Laboratory of Terahertz Technology, Ministry of Education, Chengdu 610054, China;
3. State Key Laboratory of Oral Diseases, National Clinical Research Center for Oral Diseases, West China Hospital of Stomatology, Sichuan University, Chengdu, 610041, China. ;
4. Tian Fu Jiang Xi Laboratory, Chengdu, China, 641419;E-mail:Xiaoqiuyan Zhang: zhang_xqy@uestc. edu. cn;
Li Cheng: dentistcl@scu. edu. cn;Min Hu:hu_m@uestc. edu. cn)

Abstract: Enamel demineralization often occurs in the early stage of dental caries. Studying the microscopic mechanism of enamel demineralization is essential to prevent and treat dental caries. Terahertz (THz) technology, especially continuous wave (CW) THz near-field scanning microscopy (THz-SNOM) with its nanoscale resolution, can be promising in biomedical imaging. In addition, compared with traditional THz time-domain spectroscopy (TDS), portable solid-state source as the emission has higher power and SNR, lower cost, and can obtain more precise imaging. In this study, we employ CW THz-SNOM to further break the resolution limitations of conventional THz imaging techniques and successfully achieve the near-field imaging of demineralized enamel at the nanoscale. We keenly observe that the near-field signal of the enamel significantly lowers as demineralization deepens, mainly due to the decrease in permittivi-

ty. This new approach offers valuable insights into the microscopic processes of enamel demineralization, laying the foundation for further research and treatment.

Key words: Demineralized enamel, Near-field, CW THz-SNOM
PACS:

1 Introduction

Modern dental medicine for common dental disease namely caries mainly emphasizes non-invasive treatment of caries, specifically, local treatment to prevent further caries before they form cavities, to remineralize early caries, and to restore the integrity of enamel[1]. The contribution of conventional radiographs in identifying early caries seems negligible among these detecting methods. Micro-computed tomography (Micro-CT) is suitable for caries only with large or formed cavities, thus early caries detection is not sensitive and specific enough, and the harm of X-ray cannot be neglected[2]. The accuracy of quantitative light-induced fluorescence (QLF) results can sometimes be affected by tooth scattering, surface distribution and other factors[3-4]. Optical coherence tomography (OCT) can only indirectly reflect mineral changes and lacks more intuitive and effective quantitative indicators[5]. Transverse microradiography (TMR) technology [6], considered the "gold standard," also damages samples due to X-ray exposure and fails to reveal the microstructure of enamel demineralization. Therefore, a comprehensive diagnostic technique is requisite for early caries detection and progress monitoring.

Due to the non-ionizing properties [7], good penetration capabilities and resolution [8-9], THz waves, typically ranging from 0.1 THz to 10 THz, are increasingly employed in various fields such as biomedical imaging applications[10-13], artwork conservation and evaluation[14-16], industry (nondestructive testing of coatings[17] and paints[18]) and agriculture [19-20]. THz waves' application, especially in biomedical imaging is challenging given its limitation in imaging resolution. Therefore, the THz-SNOM system [21-22] combines scattered THz spectroscopy with AFM technology, enabling nanoscale-resolution THz imaging and has been successfully used in biomedical studies such as demineralized tooth detection[23] and the investigation of THz near-field responses of single proteins[24].

This study addresses imaging resolution's limitations in detecting methods and presents a technique for early enamel demineralization detection and progression monitoring. Compared with TDS, solid-state source as the emission source is more portable, has lower cost, higher power and SNR. The CW THz-SNOM system enables the observation of enamel morphology and structural changes before and after demineralization at the microscopic level, as well as the detection of enamel composition variations. We find that tooth enamel's dielectric constant changes obviously due to its microstructure and composition change after demineralization; with the deepening of demineralization, the dielectric constant changes more violently. Although the in-situ detection of early caries is not achieved, due to its non-ionizing properties, CW THz-SNOM system will hold significant potential for enhancing early demineralization detection and treatment by uncovering the underlying mechanisms of enamel demineralization.

2 Methods and Materials

2.1 CW THz-SNOM Experiments

The setup of the CW THz-SNOM system is depicted in Fig. 1(a), with a solid-state radiation source used, namely the Impatt avalanche diode radiation source produced by TeraSense, Russia. The emitted THz wave frequency is 97.8 GHz, and the power is about 90 mW. The radiation source is compact and portable. We employ the BenYuan CSPM5500 series scanning probe microscope, and the lock-in amplifier is a Zurich Instruments MFLI series lock-in amplifier with a bandwidth reaching 5 MHz. The probe is constructed using a Rocky Mountain Nanotechnology (RMN) 25Ptlr200B-H series probe with an 80 μm tip length and a 200 μm cantilever length. The diameter of the probe tip is about 100 nm. We use the waveguide detector with a bandwidth of 75-110 GHz. The

imaging resolution is determined by the size of the probe tip rather than the wavelength, allowing the diffraction limits to be exceeded and achieving nanoscale imaging.

2.2 Sample preparation

The protocol of this study complied with the NIH Guide for the Care and Use of Laboratory Animals and was approved by the Ethics Committee of West China Dental Hospital, Sichuan University (WCHSIRB-D-2021-285). We collected fresh bovine teeth, separated the crown and root, and polished the enamel surface. The sample was then embedded in epoxy resin, leaving a highly polished surface of at least 5 x 5 mm. The sample was then placed in a prepared demineralized buffer[25-26] for 5 days. Finally, a vertical cut was made on the enamel surface to obtain the tooth slice. As shown in Fig. 1(b), the tooth slice contains demineralized, normal enamel, and dentin from top to bottom. We can find that there is a clear boundary between enamel and dentin. Early demineralization mainly occurs on the surface of enamel, and the enamel turns slightly white after demineralization.

3 Results and Discussions

As shown in Fig. 1(b), the area framed by the blue curve is selected for imaging. The scanning area is 80*80 μm, consisting of 256*256 pixels in total. This area is just the borderline between demineralized and normal enamel. Figure 1(c) and (d) display the AFM and near-field imaging results, respectively. As evident from Fig. 1(c) and (d), enamel morphology undergoes significant changes following demineralization; the fluctuations become more intense, and the near-field signal also noticeably decreases. In contrast, the near-field signal precisely represents the differences between regions before and after demineralization.

To further investigate the relationship between enamel's height fluctuations and near-field amplitude before and after demineralization, the AFM and near-field data from dashed lines in Fig. 1(c) and (d) are used to plot the curve, as shown in Fig. 1(e), the AFM height in normal enamel region fluctuates around 600-800 nm, with minimal variations. By our calculation, the average height fluctuation in normal region is 720nm with a standard deviation of 71.75, whilst

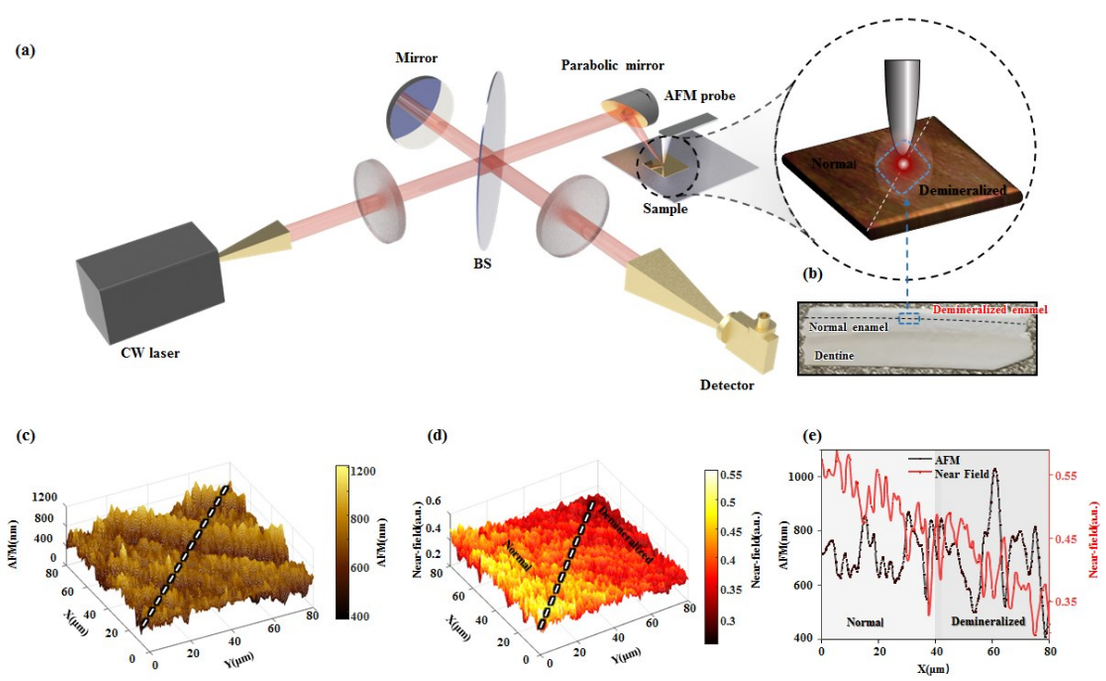

Figure1 (a) Schematic illustration of the CW THz-SNOM setup. (b) Photo of the tooth slice (the area highlighted by the blue curve is the scanning range). (c) AFM results. (d) Near-field imaging results. (e) AFM and near-field signals along the dashed line.

714nm with a standard deviation of 132.07 for demineralized region. In contrast with the intense enamel fluctuations after demineralization, mainly caused by structural change, the average height varies inapparently. The mean value of the near-field signal before demineralization is 0.498, with a standard deviation of 0.105; it then drops to 0.401 and the standard deviation alters to 0.119 after demineralization. The near-field signal exhibits a marked decrease by entering the demineralized area, but not primarily caused by height fluctuations. As the THz near-field signal can be sensitive to the sample's dielectric properties, the decrease in near-field amplitude suggests that the THz dielectric properties of enamel have significantly changed after demineralization.

We approximate the dielectric constants of the standard and demineralized regions based on the methods described in the past research[27]. A new analysis model of probe-sample interaction in s-SNOM is proposed in the article. The probe is treated as a long sphere much smaller than the wavelength, and its near field is described by a finite dipole consisting of point charges. As shown in Fig. 2(a) and (b), after demineralization, the real part (ε_1) of the enamel dielectric constant decreased from 8 to below 5, while the imaginary part (ε_2) increased from 0.5 to more than 1.2. We use the CST simulation method to further study the effect of the dielectric constant change on near-field signal change. We set the length of the near-field tip to 80 μm and the radius to 1 μm, place the tip 100 nm above the medium, determine the thickness of the medium to be 5 μm, and select the frequency of 0.1 THz. To reduce the simulation time, the apex radius of the tip chosen for the numerical simulations is larger compared to conventional SNOM tips; and would have a stronger near-field amplitude, but no obvious impact on the line profiles[28]. By changing the dielectric constant of the medium (ε_1 from 1 to 12, ε_2 from 0.5 to 1.6), we get the change in the near field signal strength, as shown in Fig. 2(c). It can be found that both increases in the real and imaginary parts of the dielectric constant can lead to the near-field signal's enhancement. Nevertheless, the effect of the real part is more significant than that of the imaginary part. Therefore, we further prove that the decrease of the near-field signal after demineralization is caused by the decrease of the dielectric constant (dominated by the real part).

To further reveal the microscopic mechanism of demineralization, we successively select 4 regions from the standard to demineralized enamel region for more detailed imaging, as depicted in Fig. 3. Figure 3(a)-(d) represent the AFM imaging results, while Fig. 3(e)-(h) illustrate the corresponding near-field imaging results. The scanning area is 30*30 μm, maintaining the 256*256 pixels resolution.

The scanning ranges in Fig. 3(a) and (b) are within the typical enamel region, while those in Fig. 3(c) and (d) are in the demineralized region, with (d) displaying a more pronounced degree of demineralization than (c). As previously described in studies[29], the basic structure of enamel is an enamel rod, which exists through the whole layer of enamel, and it is not straight in the process of shape but intertwines with

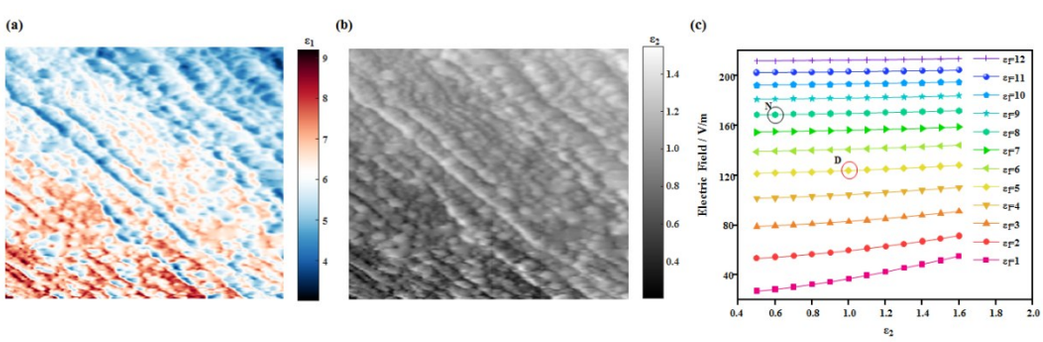

Figure2 (a) The real part of the dielectric constant of enamel. (b) The imaginary part of the dielectric constant of enamel. (c) Influence of ε_1 and ε_2 changes on near-field signal (The black circle represents normal enamel and the red represents demineralized enamel).

each other. The enamel rod diameter on the surface exceeds that at the bottom. Under an electron microscope, the cross-section of the enamel rod is racquet-shaped. The head and tail of the adjacent enamel rod are embedded. As depicted in Fig. 3(a) and (b), the standard enamel structure is organized by numerous enamel rods (indicated by the red curved area). Past studies have disclosed [23,30] the essence of demineralization involving the dissociation and remodeling of crystals, along with the transfer of mineral ions. When external substances such as acid invade the enamel, external hydrogen ions penetrate the enamel, the minerals at the front of the enamel will dissolve, and some ions such as calcium and phosphorus will diffuse and transport outwards. In this process, the structure of the enamel rod collapses, forming up and down cavities[31], and the composition of the enamel rod will also change due to the transfer of ions.

By referring to the AFM and near-field results, we observe that the enamel rod structure progressively changes in Fig. 3(e)-(h), with the most notable variations appearing in Fig. 3(h), characterized by numerous enamel rod fractures and cavity structure formations. As demineralization deepens, the near-field signal decreases further. Compared with the AFM results, the near-field imaging results highlight the impact of surface structure changes and indicate a noticeable decrease in the near-field signal of samples after demineralization, mainly due to the changes in the structure and composition of the enamel rods during the demineralization process. These changes lead to a fall-off of the enamel dielectric properties, weakening the near-field signal. We then draw the corresponding boxplot according to the AFM and near-field data of 4 regions, as shown in Fig. 3(i), illustrating the height fluctuations and the near-field amplitude changes throughout the scanning process. The mean value of AFM and near-field data in each region is calculated and connected to form the mean value line. It is observable that in the normal enamel region, the height varies between 300-400 μm, and remains relatively stable. However, in the demineralized area, the

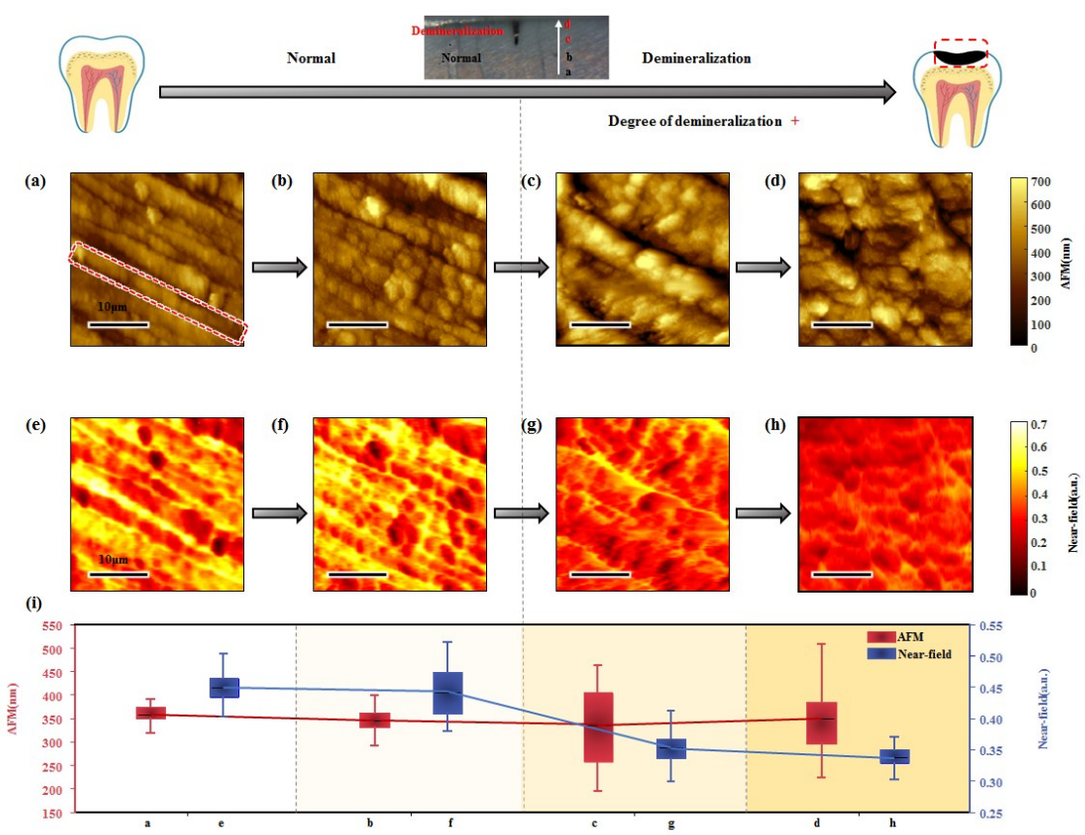

Figure3　(a)-(d) AFM results. (e)-(h) Near-field imaging results. (i) The boxplot of AFM and near-field data in each region. The black line in each box represents the mean value which is connected to form the mean value line.

height fluctuates drastically due to the alteration of surface topography, ranging between 200–500 μm.

The near–field signal strength of the normal enamel portion is considerably higher than that of the demineralized area. Moreover, the signal decrease becomes more pronounced as the degree of demineralization deepens.

To show that our findings are reliable and not related to a specific region, we randomly select several areas for scanning imaging as shown in Fig. 4. Fig. 4 (a) and (b) are in the normal region, and Fig. 4(c) and (d) are in the demineralized region. The scanning area is 40*40 μm, maintaining the 256*256 pixels resolution. The results are consistent with the previous conclusion. The structure of the enamel rod collapses in the demineralized region, and the near–field signal in the demineralized area decreases obviously. Hence, we conclude that the decrease in the near–field signal of the demineralized process is mainly caused by the reduction in dielectric properties resulting from the alteration of enamel structure and composition after demineralization.

4 Conclusion

In summary, we utilize a CW THz–SNOM system to obtain precise enamel images before and after demineralization, confirming that the changes in its structure and composition after demineralization will decrease the dielectric constant, thus weakening the near–field signal. As more advantageous than the AFM results, the near–field signal can more comprehensively reveal the microscopic mechanism of demineralization. Thus, this work provides a promising method for early demineralization detection of hard tissue of teeth. Yet, by specific limitations, we use acid corrosion of demineralized buffer to demineralize the enamel for an ideal situation, whilst in real cases, demineralization can be more complicated with multiple factors. Although we choose the solid–state radiation source wave as a THz emitter, the near–field signal is still not strong enough, making it challenging to observe the higher–order information of the near–field signal. Moreover, THz equipment's overall complexity and high–cost will affect its actual application. Meanwhile, because THz–SNOM can only be used to penetrate the thickness of the sample 100–300 nm in ordinary medium, it can not realize the in–situ measurement of early caries at present. In the future, more diversified demineralization methods can be expected shortly. The further development of THz technology, with the application of higher–power THz sources, and the emergence of more concise and low–cost THz devices will make it possible to apply THz technology in clinical stomatology.

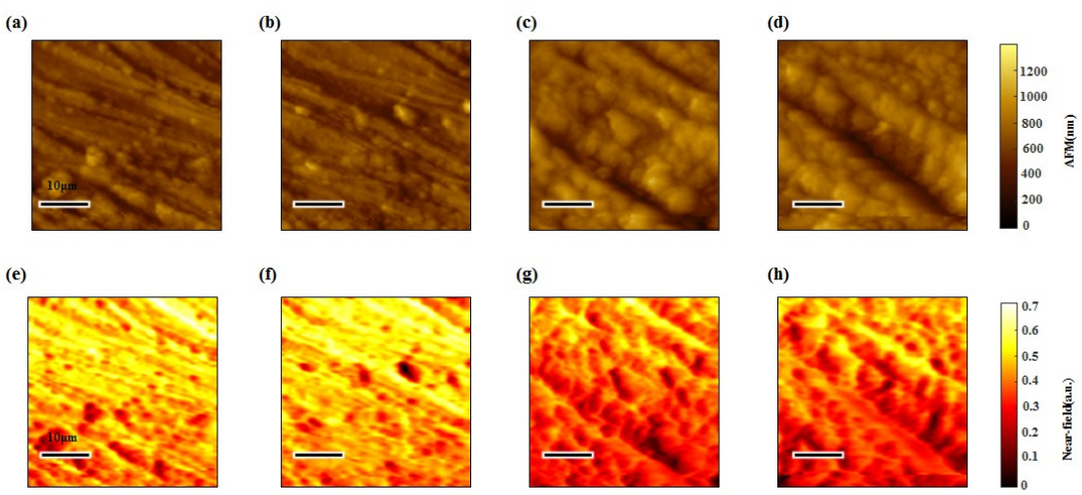

Figure4 (a)-(b) AFM results in normal enamel. (c)-(d) AFM results in demineralized enamel. (e)-(f) Near-field imaging results in normal enamel. (g)-(h) Near-field imaging results in demineralized enamel.

致 谢：Natural Science Foundation of China under Grant 61988102, 61921002 and 62071108, and the fund of Key Laboratory of THz Technology, Ministry of Education, China. The authors acknowledge the support of Chengdu Miji Technology Co., LTD.

References

[1] L. Gorelick, A.M. Geiger and A.J. Gwinnett, Incidence of white spot formation after bonding and banding, Am. J. Orthod. 81, 2 (1982).

[2] M.N. A. Bijle, E. Ekambaramlo, C.M. Yung and C.K. Yiu, The combined enamel remineralization potential of arginine and fluoride toothpaste, J dent. 76 (2018).

[3] J. Gomes, Detection and diagnosis of the early caries lesion, BMC Oral Health. 15. Suppl 1:S3 (2015.

[4] Q. Xiao, R. Tu, T. He, W. Yin, X. Li, D.Y. Hu and X.M. Zhang, Evaluation of Fluorescence Imaging with Reflectance Enhancement (FIRE) for Quantifying Enamel Demineralization In vitro, Caries Res. 49, 5 (2015).

[5] A. Aden, A. Anthony, C. Brigi, M. S. Merchant and P. H. Tomlins, Dynamic measurement of the optical properties of bovine enamel demineralization models using four-dimensional optical coherence tomography, J. Biomed. Opt. 22, 7 (2017).

[6] A. Lussi, M. Von Salis-Marincek, C. Ganss, E. Hellwig, Z. Cheaib and T. Jaeggi, Clinical study monitoring the pH on tooth surfaces in patients with and without erosion, Caries Res. 46, 6 (2012).

[7] I. Zaytsev, I. N. Dolganova, N. V. Chernomyrdin, G. M. Katyba, A. A. Gavdush, O. P. Cherkasova, G. A. Komandin, M.A. Shchedrina, A.N. Khodan and D.S. Ponomarev, The progress and perspectives of terahertz technology for diagnosis of neoplasms: A review, J. Opt. 22, 1 (2020).

[8] Z. Yan, L.G. Zhu, K. Meng, W. Huang and Q. Shi, THz medical imaging: from in vitro to in vivo, Trends in biotechnology. 40, 7 (2022).

[9] T. Amini, F. Jahangiri, Z. Ameri and M.A. Hemmatian, A Review of Feasible Applications of THz Waves in Medical Diagnostics and Treatments, J Lasers Med Sci. 12 (2021).

[10] X. Fu, Y. Liu, Q. Chen, Y. Fu, and T. J. Cui, Applications of terahertz spectroscopy in the detection and recognition of substances, Frontiers Phys. 10 (2022).

[11] P. Zhang, S.C. Zhong, J.X. Zhang, J. Ding, Z.X. Liu, Y. Huang, N. Zhou, W. Nsengiyumva and T.F. Zhang, Application of terahertz spectroscopy and imaging in the diagnosis of prostate cancer, Current Opt. Photon. 4, 1 (2020).

[12] X.Q. Chen, H. Lindley, R.I. Stantchev, J. Wang, K. Li, A. Hernandez Serrano, Z. D. Taylor, E. Castro-Camus and E. Pickwell-MacPherson, Terahertz (THz) biophotonics technology: Instrumentation, techniques, and biomedical applications, Chem. Phys. Rev. 3, 1 (2022).

[13] X. Yang, X. Zhao, Ke, Yang, Y.P. Liu, Y. Liu, W.L. Fu and Y. Luo, Biomedical applications of terahertz spectroscopy and imaging, Trends Biotechnol. 34, 10 (2016).

[14] K. Fukunaga and M. Picollo, Terahertz spectroscopy applied to the analysis of artists' materials, Appl. Phys. A, Solids Surf. 100, 3 (2010).

[15] D. Giovannacci, H.C. Cheung, G.C. Walker, J.W. Bowen, D. Martos-Levif, D. Brissaud, L. Cristofol and Y. Melinge, Time-domain imaging system in the terahertz range for immovable cultural heritage materials, Strain. 55 (2019).

[16] M. Inuzuka, Y. Kouzuma, N. Sugioka, K. Fukunaga, and T. Tateishi, Investigation of layer structure of the takamatsuzuka mural paintings by terahertz imaging technique, J. Infr., Millim., Terahertz Waves. 38, 4 (2017).

[17] L. Xing, H.L. Cui, C.C. Shi, Z.Y. Zhang, J. Zhang, T.Y. Chang, D.S. Wei, C.L. Du, S.N. Zhang and Z.X. Zhou, Nondestructive examination of polymethacrylimide composite structures with terahertz time-domain spectroscopy, Polym. Test. 57 (2017).

[18] K. Su, Y.-C. Shen, and J. A. Zeitler, Terahertz sensor for non-contact thickness and quality measurement of automobile paints of varying complexity, IEEE Trans. Terahertz Sci. Technol. 4, 4 (2014).

[19] H. Ge, Y. Jiang, and Y. Zhang, THz spectroscopic investigation of wheat-quality by using multi-source data fusion, Sensors. 18, 11 (2018).

[20] L. Hui, W. Jingzhu, L. Cuiling, S. Xiaorong, and Y. Le, Study on pretreatment methods of terahertz time domain spectral image for maize seeds, IFAC-PapersOnLine. 51, 17 (2018).

[21] G. B. Dai, Z. B. Yang, G. S. Geng, M. L. Li, T. Y. Chang, D. S. Wei, C. L. Du, H.-L. Cui and H. B. Wang, Signal detection techniques for scattering-type scanning near-field optical microscopy, Appl. Spectrosc. Rev. 53, 10 (2018).

[22] X. Z. Chen, D. B. Hu, R. Y. Mescall, G. J. You, D. N. Basov, Q. Dai, M. K. Liu, Modern scattering-type scanning near-field optical microscopy for advanced material research, Adv. Mater. 31, 24 (2019).

[23] F. Xiao, X.Q.Y. Zhang, X.X. Xu, T.Y. Zhang, F. Tang, H.W. Yin, T. Hu, L. Lei, L. Cheng and M. Hu, Unveiling enamel demineralization mechanisms by sensitive dielectric differentiation based on terahertz nanospectroscopy, Biomed. Opt. Express. 15, 9 (2024).

[24] Z. Yang, D. Tang, J. Hu, M. Tang, M. Zhang, H.L. Cui, L. Wang, C. Chang, C. Fan, J. Li and H. Wang, Near-Field Nanoscopic Terahertz Imaging of Single Proteins, Small. 17, 3 (2020).

[25] J.M. ten Cate and P.P.E. Duijsters, Influence of fluoride in solution on tooth demineralization, I. Chemical data, Caries Res. 17 (1983).

[26] Y. Yang, X.P. Lv, W. Shi, J.Y. Li, D.X. Li, X.D. Zhou and L.L. Zhang, 8DSS-promoted remineralization of initial enamel caries in vitro, J Dent Res. 93, 5 (2014).

[27] A. Cvitkovic, N. Ocelic and R. Hillenbrand, Analytical model for quantitative prediction of material contrasts in scattering-type near-field optical microscopy, Opt. Express. 15, 14 (2007).

[28] C. Maissen, S. Chen, E. Nikulina, A. Govyadinov, and R. Hillenbrand, Probes for Ultrasensitive THz Nanoscopy, ACS photonics. 6, 5 (2019).

[29] Z.R. Zhou, W. Gong and J. Zheng, Bionic design perspectives based on the formation mechanism of dental anti-

wear function, Biosurface Biotribology. 3, 4 (2018).
[30] Y. Lei, T. Wang J.W. Mitchell, L. Zaidel, J. Qiu and L. Kilpatrick-Liverman, Bioinspired amphiphilic phosphate block copolymers as non-fluoride materials to prevent dental erosion, RSC Advances. 4, 90 (2014).
[31] F. Yun, M. V. Swain, H. Chen, J. Cairney, J. Qu, G. Sha, H. Liu, S. P. Ringer, Y. Han, L. Liu, X. Zhang, and R. Zheng, Nanoscale pathways for human tooth decay – Central planar defect, organic-rich precipitate and high-angle grain boundary. Biomaterials. 235 (2020).